The Effect of Tungsten on Dislocation Recovery and Precipitation Behavior of Low-Activation Martensitic 9Cr Steels

F. ABE, H. ARAKI, and T. NODA

The effect of W on dislocation recovery and precipitation behavior was investigated for martensitic 9Cr-(0,1,2,4)W-0.1C (wt pct) steels after quenching, tempering, and subsequent prolonged aging. The steels were low induced-radioactivation martensitic steels for fusion reactor structures, intended as a possible replacement for conventional (7 to 12)Cr-Mo steels. During tempering after quenching, homogeneous precipitation of fine W_2C occurred in martensite, causing secondary hardening between 673 and 823 K. The softening above the secondary hardening temperature shifted to higher temperatures with increasing W concentration, which was correlated with the decrease in self-diffusion rates with increasing W concentration. Carbides $M_{23}C_6$ and M_7C_3 were precipitated in the 9Cr steel without W after high-temperature tempering at 1023 K. With increasing W concentration, M_7C_3 was replaced by $M_{23}C_6$, and M_6C formed in addition to $M_{23}C_6$. During subsequent aging at temperatures between 823 and 973 K after tempering, the recovery of dislocations, the agglomeration of carbides, and the growth of martensite lath subgrains occurred. Intermetallic Fe_2W Laves also precipitated in the δ-ferrite grains of the 9Cr-4W steel. The effect of W on dislocation recovery and precipitation behavior is discussed in detail.

I. INTRODUCTION

TEMPERED martensitic steels, such as modified 9Cr-1Mo (9Cr-1Mo-0.2V-0.08Nb-0.1C) and HT-9 (12Cr-1Mo-0.5W-0.3V-0.5Ni-0.2C), are being considered as candidate structural materials for fusion reactors because of their excellent swelling resistance compared with austenitic stainless steels.[1] Recently, however, in order to simplify special waste storage of the highly radioactive blanket and first-wall structures from fusion reactors after service, the development of low activation steels has received attention.[2] In low activation steels, the concentration of Mo, Nb, and Ni, which are principal alloying elements in conventional Cr-Mo steels, such as modified 9Cr-1Mo and HT-9, must be severely restricted. These elements transmute into long-lived radioactive nuclides when they are irradiated with the high-energy neutrons (10 to 14 MeV) found in the first-wall and blanket structure.[3] Alloying elements that can be used in low activation steels include C, W, V, Ta, Ti, Mn, and Si. At present, Cr-W steels offer the best possibility for the base composition of low activation ferritic/martensitic steels that can replace conventional Cr-Mo steels.

Although the irradiation response, including irradiation hardening, irradiation embrittlement, and irradiation-induced microstructural evolution, of these newly developed Cr-W steels is now being extensively studied,[4,5,6] research on the physical metallurgy of unirradiated material is still insufficient.[7,8,9] Tempered martensitic steels usually consist of lath subgrains which contain a high density of dislocations or dislocation network and fine carbides, depending on tempering temperature. However, δ-ferrite can also form during austenitizing, and some steels can form intermetallic phases during tempering as well. These microstructural constituents significantly affect the mechanical properties of tempered martensitic steels. Therefore, it is important to understand the effect of W on microstructural evolution in martensitic Cr-W steels.

The purpose of the present research is to investigate systematically the effect of W on dislocation recovery and precipitation behavior of carbides and intermetallic compound in martensitic 9Cr steels containing from 0 to 4 wt pct W. Microstructural observations using transmission electron microscopy (TEM) were made after quenching, after tempering, and after prolonged aging. Hardness measurements were also made to study the secondary hardening and softening that occur during tempering of quenched material. The effect of W on microstructural evolution is comprehensively discussed.

II. EXPERIMENTAL PROCEDURE

The chemical composition of the steels examined is given in Table I. Only the concentration of W was varied from 0 to 4 wt pct in the steels, while the other alloying elements were kept constant (0.1 wt pct C, 9 Cr, 0.5 Mn, and 0.3 Si). These steels are designated 9Cr, 9Cr-1W, 9Cr-2W, and 9Cr-4W steels. The steel rods were prepared by vacuum melting in a high-frequency induction furnace to ingots of 17 kg, homogenizing at 1473 K for 1 day, hot forging to a 60-mm^2 cross section size, then hot rolling through rectangular grooves into square rods 13 mm on a side. The steels rods were cut into pieces about 20 mm in length using a water-cooled fine cutter and then heat-treated. First, the steel rods were austenitized and quenched and then followed by tempering experiments. The quenching temperatures were

F. ABE, Senior Researcher, H. ARAKI, Researcher, and T. NODA, Head of the Second Laboratory, are with the Second Research Group (Nuclear Materials), National Research Institute for Metals, Tsukuba Laboratories, Tsukuba 305, Japan.

Manuscript submitted October 22, 1990.

Table I. Chemical Composition of Steels Examined (Weight Percent)

Steels	C	Cr	W	Mn	Si	P	S	O	N
9Cr	0.104	8.96	—	0.49	0.30	<0.002	0.003	0.009	0.001
9Cr-1W	0.101	9.01	0.99	0.48	0.29	<0.002	0.004	0.011	0.002
9Cr-2W	0.100	8.92	1.92	0.48	0.28	<0.002	0.003	0.012	0.002
9Cr-4W	0.101	9.09	3.93	0.50	0.29	<0.002	0.002	0.006	0.002

determined so that the prior austenite grain size was the same for all of the steels, and they are listed in Table II. In this investigation, the microstructural evolution was examined with constant grain size, because grain size is known to affect the mechanical properties of steels. The mechanical properties of the steels will be presented in another article. The annealing time at the austenitizing temperature was 3.6 ks. The average prior austenite grain size was about 50 μm. The tempering experiment was carried out between 373 and 1073 K, with a time of 3.6 ks at each tempering temperature. The hardenability of the steels during tempering was examined by measuring the Vickers hardness of the martensite phase at room temperature. The indentation load was 200 g. Subsequent prolonged aging was carried out at temperatures between 823 and 973 K for 3.6 to 10,800 ks, after appropriate tempering at high temperatures between 1023 and 1073 K.

The microstructural observations were carried out using a JEM (Japan Electron Microscope)-200CX transmission electron microscope at 200 kV. The thin foils for TEM observation were prepared by cutting thin sheets of about 0.5 to 1 mm in thickness from the specimens parallel to the rolling direction using a water-cooled fine cutter, mechanically polishing on emery papers to about 0.2 mm in thickness, and finally electrolytically polishing in an electrolyte consisting of 90 pct acetic acid and 10 pct perchloric acid. The identification of precipitates was carried out by selected area electron diffraction in TEM and by X-ray diffraction on electrolytically extracted residues. The residues were obtained by passing the electrolytic solution through a filter with 0.1-μm mesh. X-ray diffraction was carried out by using Cu K_α (λ = 0.15405 nm) radiation.

III. RESULTS AND DISCUSSION

A. *Microstructure after Quenching*

Figure 1 shows the microstructure of the steels after quenching. The 9Cr, 9Cr-1W, and 9Cr-2W steels consisted of martensite phase only, while the 9Cr-4W steel was dual phase with martensite and δ-ferrite. The critical concentration of W for the formation of δ-ferrite in the 9Cr steel with 0.1C was estimated to be about 3 pct.[10] The critical concentration of W at the austenite/(austenite + ferrite) phase boundary of the Fe-Cr-W ternary system without carbon is about 0.8 pct close to 1273 K when the concentration of Cr is 9 pct.[11] Martensite formed from austenite during quenching, whereas the δ-ferrite present at the austenitizing temperature remains. Therefore, the addition of 0.1 pct C to the 9Cr-W steels stabilizes the austenite phase at high temperatures and increases the critical concentration of W from about 0.8 to 3 wt pct.

The martensite phase consists of lath martensite subgrains containing a high density of dislocations which were produced by the martensitic phase transformation during quenching. The lath width averages about 0.5 μm, which was fairly similar among the steels. In Figure 1(d) of the dual-phase 9Cr-4W steel, the upper part is martensite phase and the lower one is δ-ferrite. The volume fraction of the δ-ferrite in the 9Cr-4W steel was 10 pct. The δ-ferrite was arranged in a bamboo structure, with a bamboo diameter of about 5 μm. The bamboo was distributed parallel to the rolling direction. The δ-ferrite contained a much lower density of dislocations, because the δ-ferrite was present at both high and low temperatures without any transformation. No precipitate was observed in either the martensite or the δ-ferrite. This indicates that all of the carbon atoms were in supersaturated solid solution during quenching. The concentrations of Cr and W in the martensite and δ-ferrite phases of the 9Cr-4W steel were analyzed by X-ray energy-dispersive specroscopy (XEDS) to be 8.5 pct Cr-3 pct W for the martensitic phase and 10 pct Cr-6 pct W for the δ-ferrite phase, indicating at least that the ferrite-forming elements Cr and W were enriched in the δ-ferrite phase.

B. *Secondary Hardening, Dislocation Recovery, and Carbide Precipitation during Tempering*

Figure 2 shows the Vickers hardness of the martensite phase of the steels as a function of tempering temperature. The steels, except for the 9Cr steel without W,

Table II. Heat-Treatment Conditions, Matrix, and Precipitates*

	QT (K)	TT (K)	Matrix	Vol Pct of δ-ferrite	Precipitates in As-Tempered	Precipitates after Aging (837 K, 3600 ks)
9Cr	1203	1023	martensite	0	$M_{23}C_6$, M_7C_3	$M_{23}C_6$
9Cr-1W	1223	1023	martensite	0	$M_{23}C_6$	$M_{23}C_6$
9Cr-2W	1223	1023	martensite	0	$M_{23}C_6$	$M_{23}C_6$
9Cr-4W	1273	1073	martensite, δ-ferrite	10	$M_{23}C_6$, M_6C	$M_{23}C_6$, M_6C, Fe_2W

*QT = quenching temperature; TT = tempering temperature.

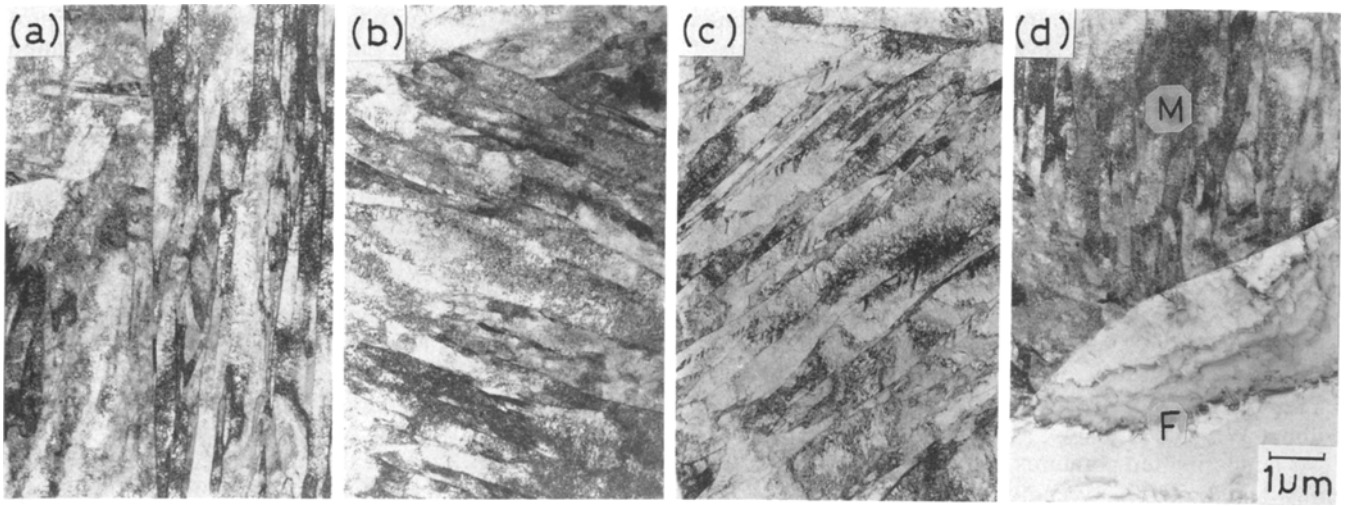

Fig. 1—Microstructure of 9Cr-W steels after quenching: (*a*) 9Cr, (*b*) 9Cr-1W, (*c*) 9Cr-2W, and (*d*) 9Cr-4W. The symbols "M" and "F" in (d) denote martensite and δ-ferrite phases, respectively.

exhibit a small secondary hardening at temperatures between 673 and 823 K. Figure 3 shows the microstructure of the 9Cr-4W steel after tempering at 773 K for 3.6 ks. The precipitation of W_2C occurred uniformly in the matrix, which was also typical for the 9Cr-1W and 9Cr-2W steels. The precipitate W_2C is known to have a hexagonal close-packed unit cell of a = 0.30 nm and c =

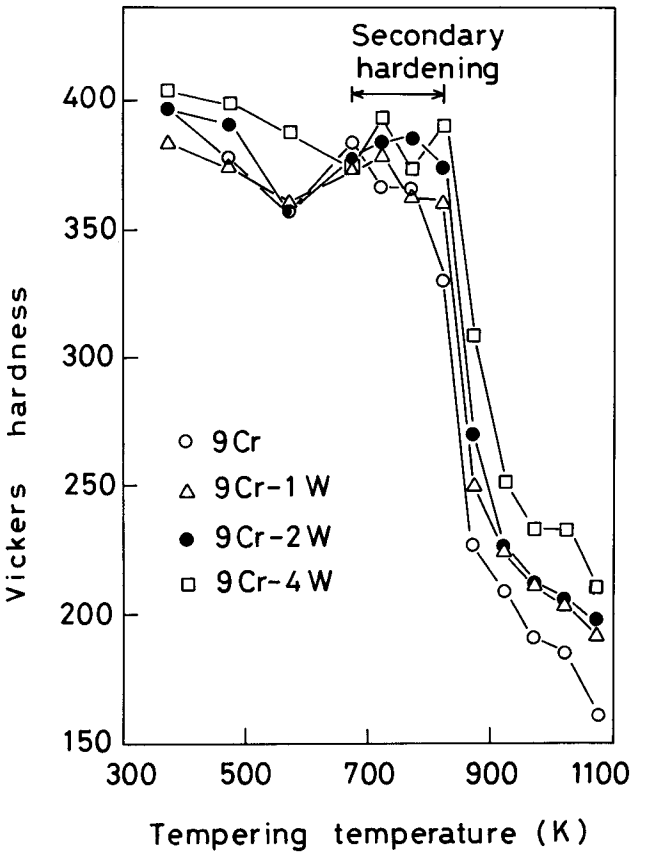

Fig. 2—Tempering curves of hardness of the steels as a function of tempering temperature. The annealing time was 3.6 ks in each step.

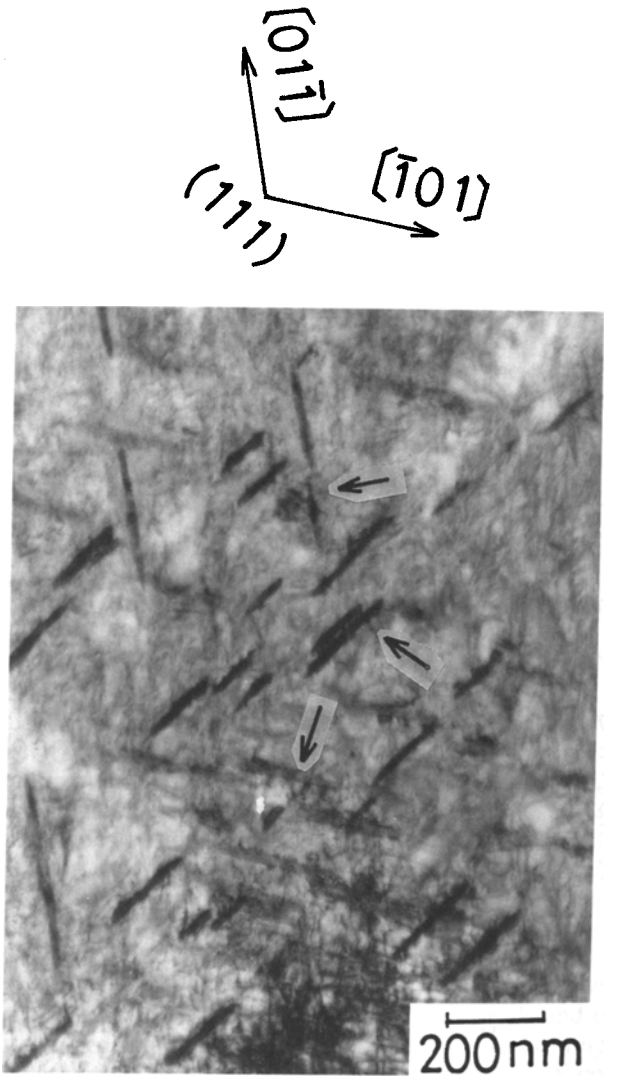

Fig. 3—Microstructure of 9Cr-4W steel after tempering at 773 K for 3.6 ks. The electron beam was perpendicular to the (111) plane of the bcc matrix. The arrows show needlelike W_2C precipitates.

0.47 nm. The W_2C precipitates are most likely responsible for the secondary hardening in the 9Cr-W steels. In Mo steels, the formation of Mo_2C is known to cause secondary hardening.[12] In Figure 3, the high density of dislocations produced by martensitic transformation during quenching still remained after this tempering treatment, and the W_2C precipitates were observed to possess a needlelike morphology, about 200-nm long and 30 to 40 nm in diameter. The needle axis of the precipitates was parallel to $\langle 110 \rangle$ directions lying in the $\{111\}$ planes of the body-centered cubic (bcc) matrix. The orientation relationship between W_2C and matrix was found to be $(0001)_{W_2C} // (111)_{bcc}$ and $[\bar{1}011]_{W_2C} // [01\bar{1}]_{bcc}$. Secondary hardening was not clearly observed in the 9Cr steel without W.

At tempering temperatures above the secondary hardening temperature, softening abruptly occurred. Softening was delayed until higher temperatures were reached in steels with more W. Figure 4 shows the tempering temperature at which the hardness decreased to 300 and 250 VHN (Vickers hardness number) as a function of W concentration. The tempering temperature corresponding to the softening temperature increases almost linearly with W concentration. The temperature shift of the softening indicates that recovery processes were being delayed with increasing W concentration. Previous work has indicated that the resistance to softening did not depend on the Cr concentration for Cr-2W steels with between 2 and 12 pct Cr.[9]

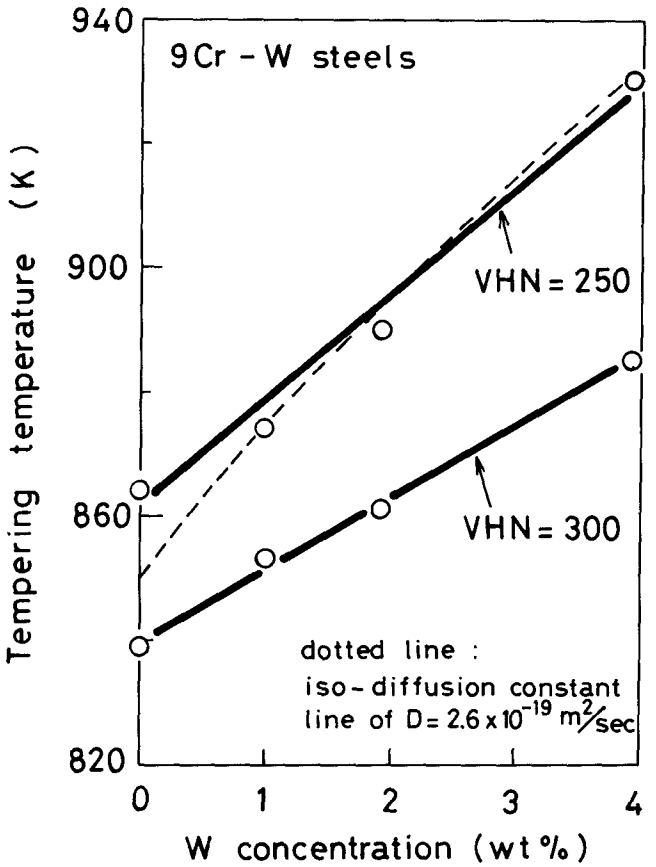

Fig. 4—Tempering temperature to 250 and 300 VHN as a function of W concentration. The dotted line shows iso-diffusion constant line of 2.6×10^{-19} m^2/s.

The softening occurred as the excess dislocations produced by the quench-induced martensitic transformation recovered during tempering. The recovery of excess dislocations occurs by dislocation climb, interacting with the carbides and other dislocations. The rate-determining process of the softening due to dislocation climb is considered to be self-diffusion mainly. However, diffusion data of 9Cr-W steels have not been reported, although those for bcc Fe-W and Fe-Cr binary systems are available. The rate of Fe diffusion in 9Cr-W steels is approximated substantially by that of the Fe-W binary alloys, because Cr has almost no effect on the diffusivity of Fe in Fe-Cr binary alloys below 10 pct Cr.[13] It is reported that W markedly decreases the rate of Fe diffusion in Fe-W binary alloys. The pre-exponential factor, D_0, and activation energy, Q, of the diffusion constant $D = D_0 \exp(-Q/RT)$ for Fe in an Fe-W binary alloy change with W concentration as follows: $D_0 = 1.5 \times 10^{-6}$, 9.3×10^{-6}, and 1.4×10^{-4} m^2/s and $Q = 210$, 230, and 255 kJ/mol for 0.15, 0.33, and 0.78 at. pct W, respectively, all of which were measured at temperatures between 958 and 1033 K.[14] Using these diffusion parameters, the W concentration dependence of the pre-exponential factor and activation energy is represented approximately as $D_0 = 6.6 \times 10^{-7} \times 10^{3.18 C_W}$ m^2/s and $Q = 202 + 72.5 C_W$ kJ/mol, where C_W denotes the concentration of W in at. pct. The relationship between at. pct W and wt pct W in a 9Cr-0.1C steel (wt pct) is given by [at. pct W] = 0.31 [wt pct W]. This permits the iso-diffusion constant line of $D = 2.6 \times 10^{-19}$ m^2/s, which corresponds to the temperature of 850 K for the 9Cr steel with 0 pct W, to be drawn as the dotted line shown in Figure 4. The iso-diffusion constant line shifts to higher temperatures with increasing W concentration, because the diffusion constant of Fe decreases with increasing W concentration. It should also be noted that the W concentration dependence of the softening temperature is similar to that of diffusion constant of Fe in Fe-W binary. This suggests that the addition of W to 9Cr steel retards the softening, because the self-diffusion rate of Fe decreases.

Martensitic steels are commonly used after tempering at temperatures of 923 to 1073 K. Tempered martensitic steels tend to have satisfactory ductility at ambient temperature and a stable microstructure during exposure to temperatures up to 773 to 823 K. In this investigation, the tempering temperature was determined by the softening characteristics such that all of the steels had about the same level of hardness (about 200 VHN). Equivalent hardness was chosen as a criterion, because the hardness level usually reflects the mechanical properties of the steels (mechanical properties measurements will be reported in another article). The tempering temperature is listed in Table II.

The microstructure of the various steels was compared after tempering at conditions that produced equivalent softening. Figure 5 shows the microstructures of the steels after tempering at the conditions given in Table II. In each steel, considerable recovery of excess dislocations has occurred. The carbides, about 0.1 μm in size, have precipitated preferentially along lath boundaries and prior austenite grain boundaries of the tempered-martensite. The W_2C precipitates which formed near 773 K in the

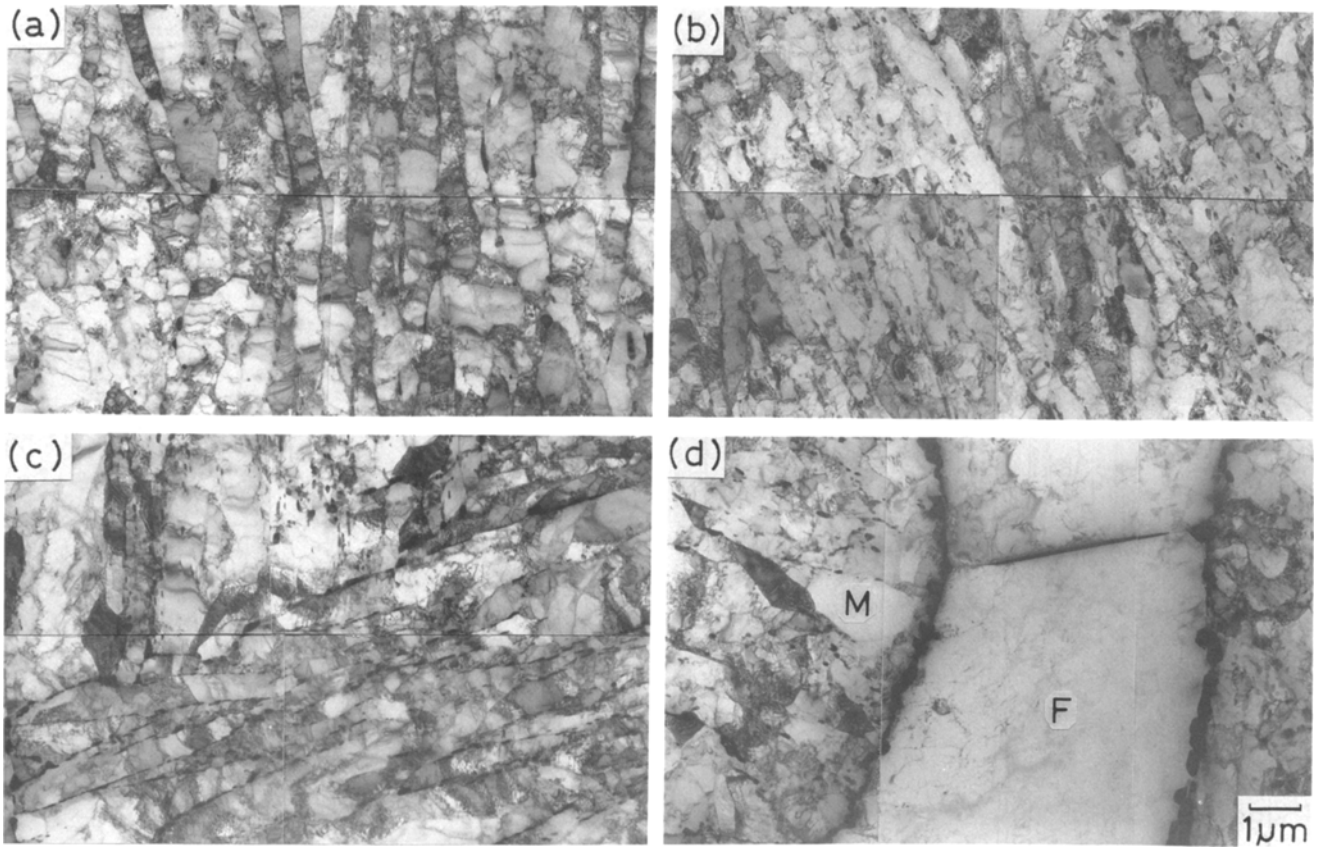

Fig. 5—Microstructure of 9Cr-W steels after tempering. The tempering temperature is listed in Table II: (*a*) 9Cr, (*b*) 9Cr-1W, (*c*) 9Cr-2W, and (*d*) 9Cr-4W. The symbols "M" and "F" in (d) denote martensite and δ-ferrite phases, respectively.

matrix have disappeared and been replaced by the $M_{23}C_6$ carbides which are more stable at higher temperatures. In the dual-phase 9Cr-4W steel, the carbides have also precipitated along tempered-martensite/δ-ferrite boundaries and δ-ferrite/δ-ferrite boundaries. However, no carbides were observed within the δ-ferrite grains themselves. The carbides found in the 9Cr-4W steel were $M_{23}C_6$ and M_6C. The $M_{23}C_6$ carbides distributed themselves uniformly in the tempered-martensite phase, while the M_6C carbides formed preferentially at the tempered-martensite/δ-ferrite and the δ-ferrite/δ-ferrite interfaces. This may well have been due to the concentration of W being lower in the tempered-martensite and higher in the δ-ferrite phase, because the formation of M_6C requires a higher concentration of W than does $M_{23}C_6$.

The lack of $M_{23}C_6$ or M_6C carbides in the δ-ferrite either suggests that the concentration of carbon in the δ-ferrite is much lower than in the tempered-martensite or that the carbon supersaturation is lower in the δ-ferrite. Therefore, little or no change in hardness occurs in the δ-ferrite during tempering. Carbon is significantly less soluble in δ-ferrite than in the austenite during high-temperature solution treating. In an iron-carbon binary system, the maximum solid solubility of carbon in the ferrite phase is only 0.02 pct at the A_1 temperature of 996 K, which is much lower than that of 2.06 pct (at 1420 K) in the austenite phase.[15] In the present case, the ferrite phase present at the austenitizing temperature is retained at room temperature, while the austenite converts to martensite during quenching. Since carbon is not likely to redistribute during quenching, the carbon concentration in the δ-ferrite is appreciably lower than in the martensite phase, which explains why the $M_{23}C_6$ or M_6C forms in the latter. When the steels contain strong carbide-forming elements, such as V and Nb, V_4C_3 and NbC carbides can form even in the δ-ferrite during tempering.[10] This suggests that the solubility of the δ-ferrite phase for carbon is indeed quite low.

The identification of the carbides by X-ray diffraction measurements made on the extracted precipitate residues is shown in Figure 6. The carbides were identified as $M_{23}C_6$ and M_7C_3 for the 9Cr steel, only $M_{23}C_6$ for the 9Cr-1W and 9Cr-2W steels, and $M_{23}C_6$ and M_6C for the 9Cr-4W steel. The majority carbide was $M_{23}C_6$ in each steel. Figure 7 shows the amount of the extracted residues of the steels, which corresponds to the amount of the carbides, as a function of W concentration. The amount of the extracted residues corresponds to the amount of carbides larger than 0.1 μm, because the mesh size of filter used in the present experiment was 0.1 μm. Most of the carbides observed with TEM in the steels had a size of about 0.1 μm after tempering. The extraction method gives us a measure of the amount of carbides in the steels and a way of quantitatively evaluating relative changes among the various steels and between aged and unaged specimens. In Figure 7, the weight percent of the carbides increases with increasing W concentration, although the carbon concentration was the same (0.1 pct) in each steel, as given in Table I. This indicates that the concentration of W in the $M_{23}C_6$ carbides

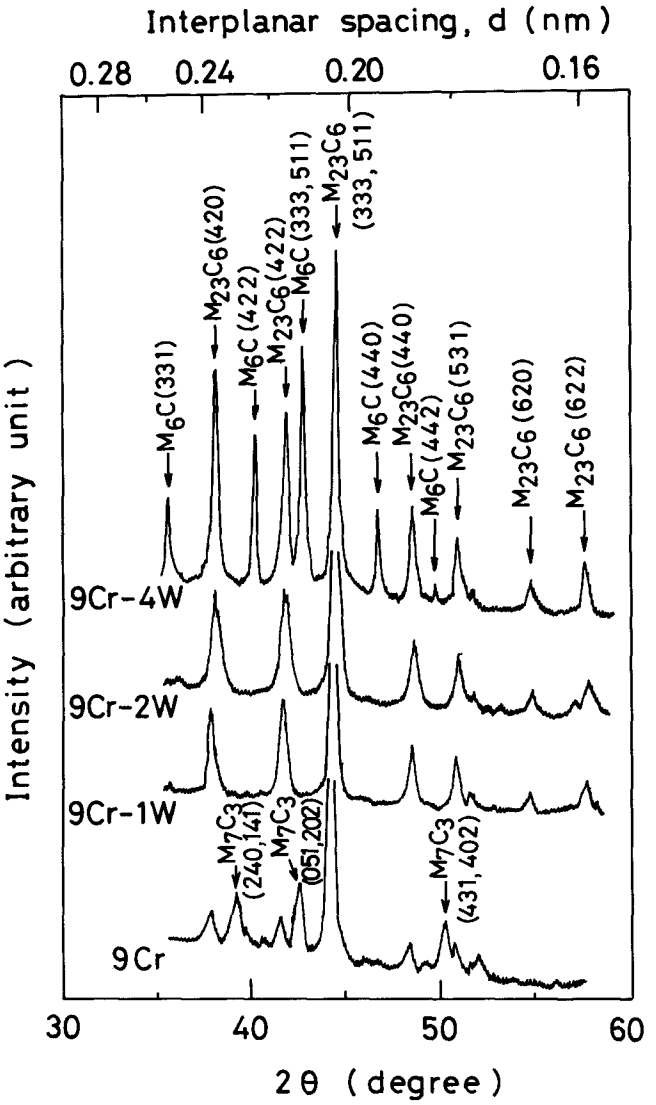

Fig. 6—X-ray diffraction patterns on extracted residues of 9Cr-W steels after tempering. The tempering temperature is listed in Table II.

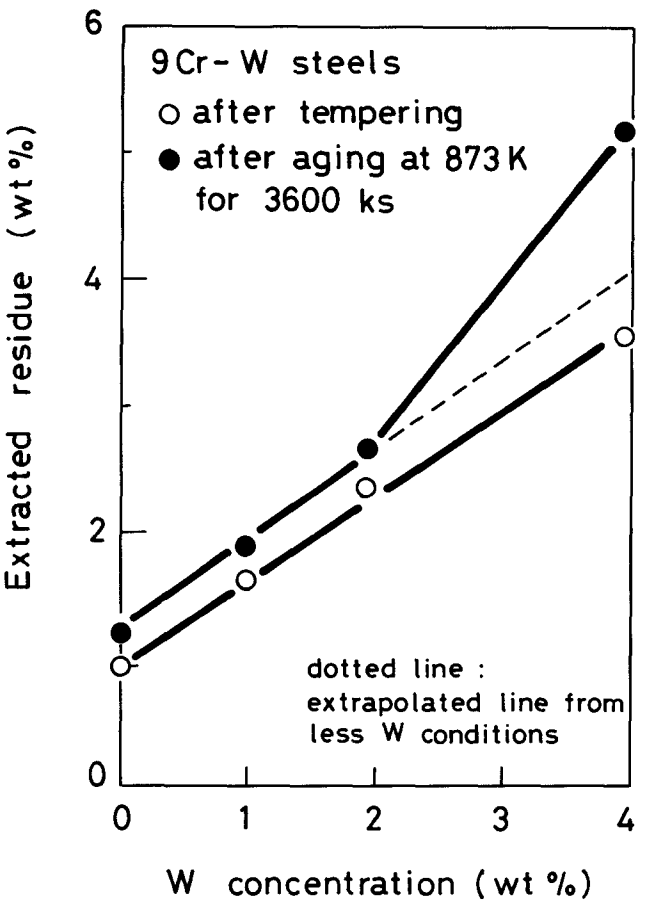

Fig. 7—Amount of extracted residues of 9Cr-W steels after tempering and after aging at 873 K for 3600 ks. The dotted line shows extrapolated line from less W conditions after aging.

increases with increasing the concentration of W in the steels. Furthermore, in the 9Cr-4W steel, M_6C containing a higher concentration of W was also formed in addition to $M_{23}C_6$.

C. *Microstructural Evolution during Aging*

After tempering at the high temperatures given in Table II, prolonged aging was carried out at temperatures between 823 and 973 K, and the microstructural evolution was examined. Figure 8 shows the microstructure of the 9Cr-1W steel after aging at 823, 873, 923, and 973 K for 10,800 ks (3000 hours). Only $M_{23}C_6$ precipitates were identified in the 9Cr-1W steel using X-ray diffraction of extracted residues after aging, the same as found after tempering. With increasing aging temperature, the density of dislocations in the matrix decreased, the $M_{23}C_6$ carbides located preferentially along lath boundaries coarsened and coalesced, and the martensite-lath subgrains grew. The dislocation recovery and carbide coarsening appear mutually related. The dislocation recovery may accelerate the carbide agglomeration. Dislocations and subgrain boundaries provide the nucleation sites and stabilize the carbides against resolution and agglomeration and, hence, against changes in the carbide distributions. On the other hand, carbides can exert pinning force on dislocations and on subgrain boundaries, suppressing dislocation recovery. The preferential distribution of the carbides along martensite lath boundaries was observed to change during aging to random distributions within the subgrains with associated carbide agglomeration. After aging at 973 K, most lath boundaries were not associated with carbide precipitates, and the larger and spheroidized carbides (about 1 μm in size) were randomly distributed. The carbide-free lath boundaries are thought to migrate easily during aging, because the carbides no longer pin the boundaries. Therefore, once the carbides dissolve and the lath boundaries break free from the carbides, the lath subgrains of the tempered-martensite grow rapidly.

Figure 9 compares the microstructure of the various steels after aging at 923 K for 10,800 ks (3000 hours). With increasing W concentration, dislocation recovery and martensite lath subgrain growth are suppressed. The preferential association between the carbides and the lath boundaries become pronounced. In the 9Cr steel without

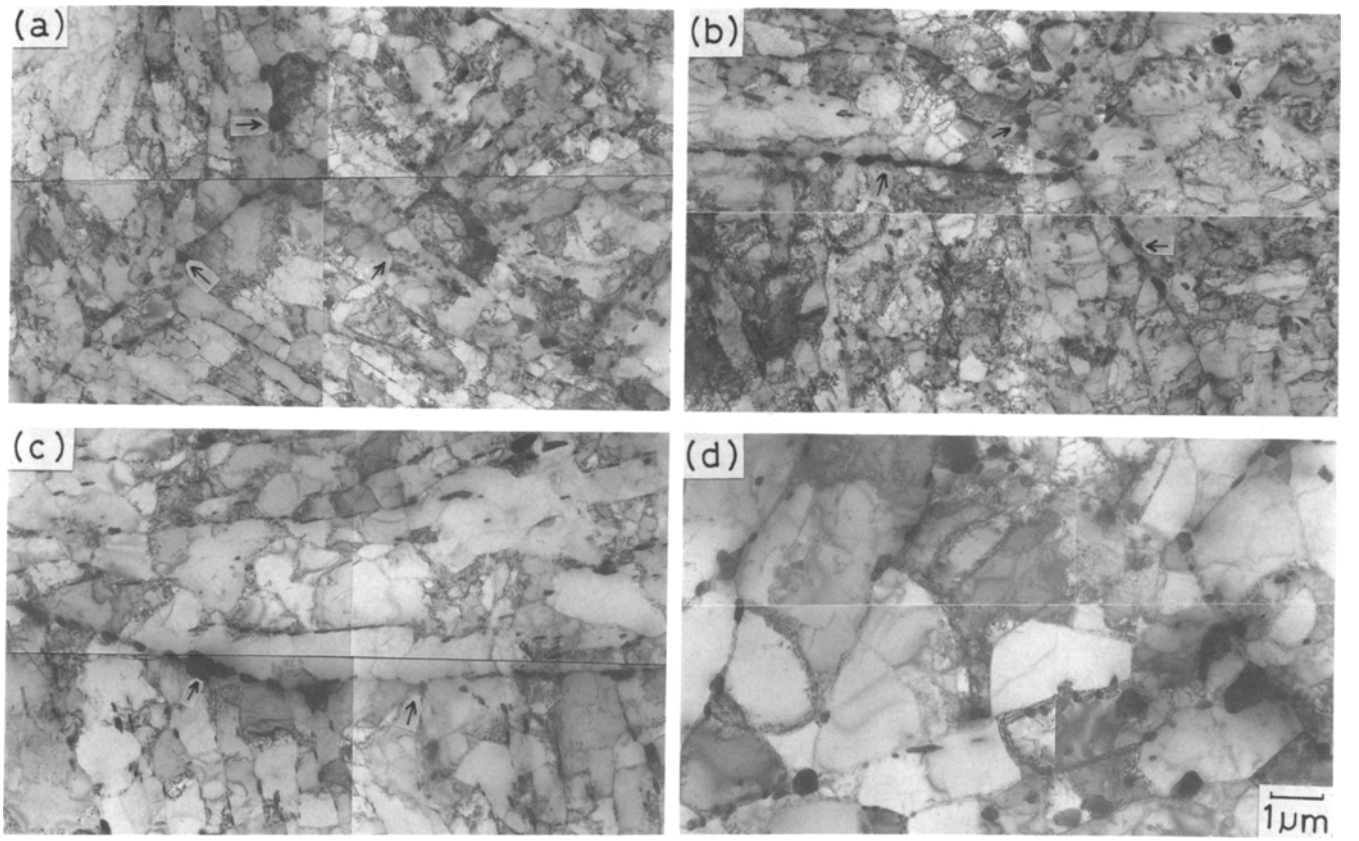

Fig. 8—Microstructure of 9Cr-1W after aging for 10,800 ks (3000 h): (*a*) 823, (*b*) 873, (*c*) 923, and (*d*) 973 K. The arrows show prior austenite grain boundaries.

W, the dislocation density in the matrix decreased considerably, and there is little association between the carbide particles and the lath boundaries. The precipitates identified by the X-ray diffraction of extracted residues in the aged steels were $M_{23}C_6$ in the 9Cr, 9Cr-1W, and 9Cr-2W steels and $M_{23}C_6$, M_6C, and Fe_2W Laves phase in the 9Cr-4W steel. The as-tempered Cr_7C_3 carbides in the 9Cr steel (Table II) dissolved during aging and were replaced by the more stable $M_{23}C_6$ carbides.

The width of the lath subgrains provides a measure of the stability of lath microstructure during aging. The size of the tempered-martensite laths increases with increasing aging temperature or with decreasing W concentration. Figure 10 shows the width of tempered-martensite laths of the steels after aging for 10,800 ks (3000 hours), as a function of aging temperature. There was considerable grain growth only in the 9Cr steel without W. There was little grain growth, and hence, little difference, among the 9Cr-1W, 9Cr-2W, and 9Cr-4W steels. A correlation between the high-temperature creep-rupture strength of the martensitic steels and the stability of the martensite lath microstructure during high-temperature exposure has been reported previously.[16] In this case, carbides were effectively associated with the lath boundaries. Coarsening of the lath subgrain structure is related to the recovery of dislocations and the agglomeration of the carbides. The recovery of dislocations is controlled by self-diffusion. The agglomeration of their carbides is related to their stability. The data presented here suggest that an increase in W concentration of the $M_{23}C_6$ phase may actually stabilize these carbides. Thus, the role of W in these steels in suppressing the growth of martensite lath subgrains appears to be through decreasing the self-diffusion rate and increasing the stability of the $M_{23}C_6$ phase.

Extensive precipitation of Fe_2W Laves phase occurred in the δ-ferrite grains but not in the tempered-martensite phase of the 9Cr-4W steel. Figure 11 shows the microstructure of the δ-ferrite phase of the 9Cr-4W steel after aging at 873 K for 3600 ks. A large number of precipitates are formed within the δ-ferrite grains, but there is a precipitate-denuded zone near the tempered-martensite/δ-ferrite interface. No precipitates were observed in the δ-ferrite grains after tempering, as shown in Figure 5. The precipitates were identified as the Fe_2W Laves phase, having a hexagonal close-packed (hcp) unit cell using both selected area electron diffraction on thin-foil specimens (Figure 12) and X-ray diffraction on extracted residues. The orientation relationship between Fe_2W Laves phase and bcc matrix was found to be $(10\bar{1}0)_{Fe_2W}//(111)_{bcc}$ and $[0\bar{1}10]_{Fe_2W}//[\bar{1}01]_{bcc}$. The Fe_2W Laves phase is known to degrade the toughness of martensitic steels. In 9Cr-Mo steels, Fe_2Mo Laves phase is known to precipitate extensively in the δ-ferrite phase.[17] In Fe-W binary system, the solid solubility of W in equilibrium with an Fe_2W second phase is reported to be about 4 wt pct at 873 K and 8 wt pct at 1073 K.[11] The concentrations of W measured in the 9Cr-4W steel were about 6 wt pct in the δ-ferrite and about 3 wt pct in the tempered-martensite phase. Therefore, the precipitation of Fe_2W

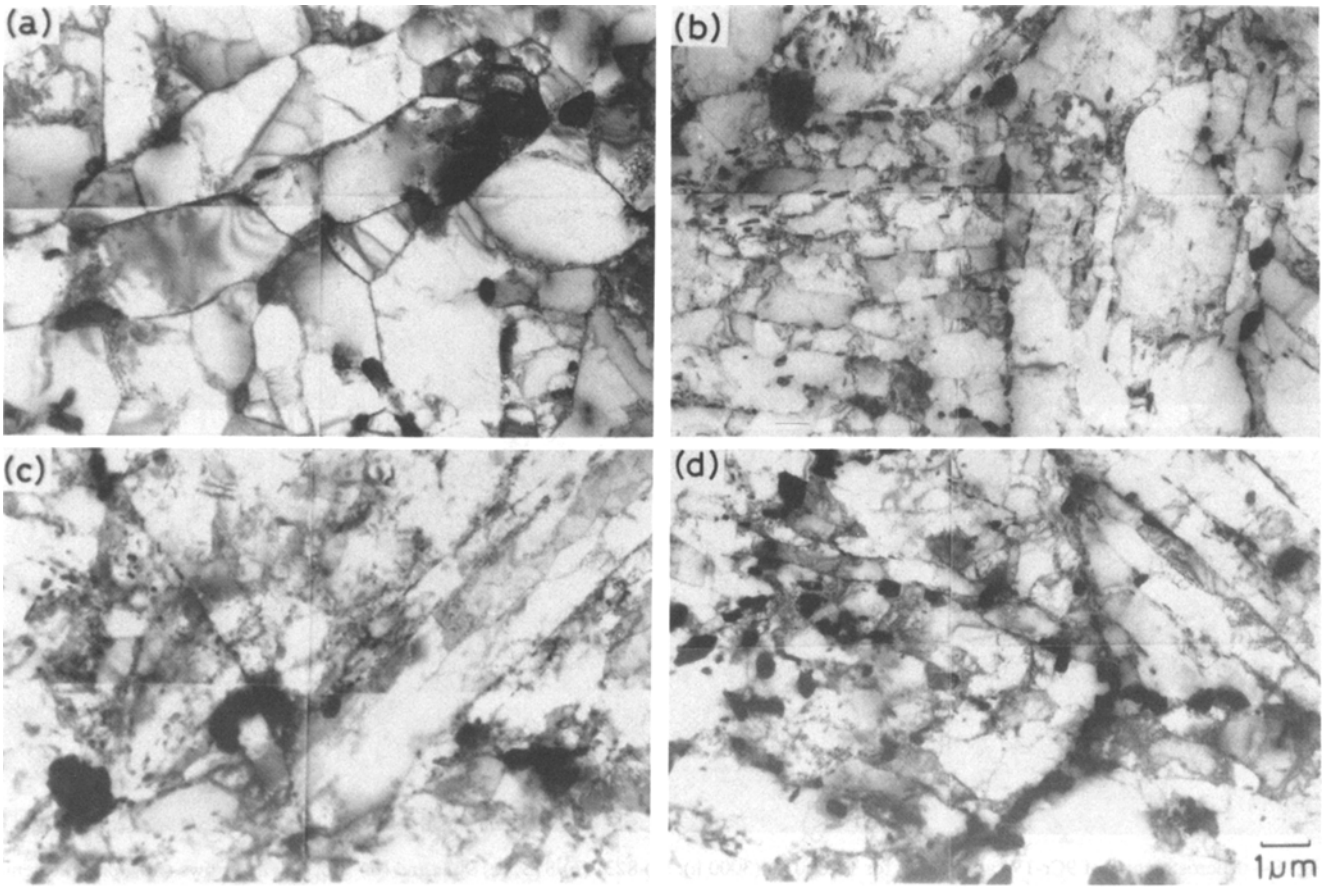

Fig. 9—Microstructure of 9Cr-W steels after aging at 923 K for 10,800 ks (3000 h): (*a*) 9Cr, (*b*) 9Cr-1W, (*c*) 9Cr-2W, and (*d*) 9Cr-4W.

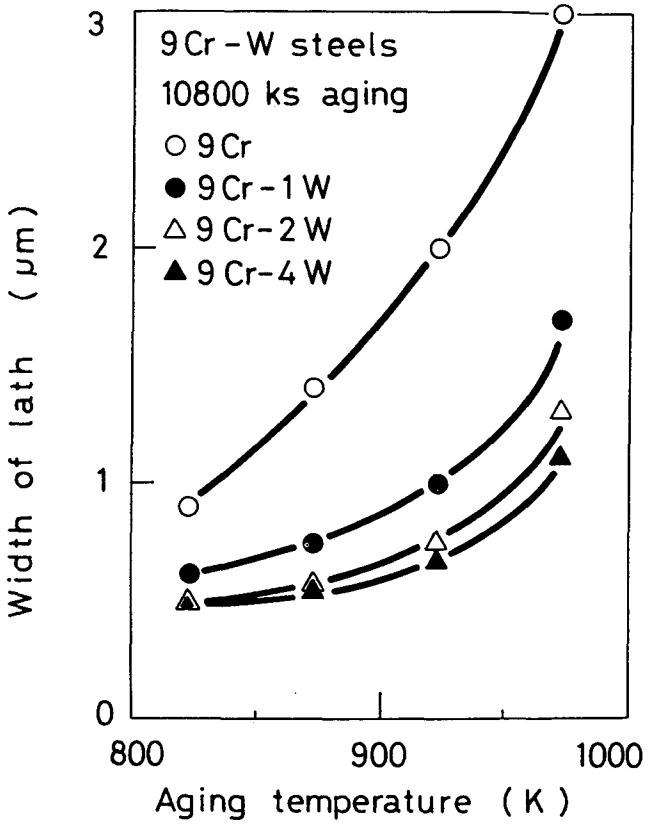

Fig. 10—Width of martensite lath of 9Cr-W steels after aging for 10,800 ks (3000 h) as function of aging temperature.

in the δ-ferrite but not in the tempered-martensite phase during aging at 873 K and the lack of Fe_2W in either phase during tempering at 1073 K are consistent with the previous solubility data on the Fe-W system. In Figure 11, the Fe_2W denuded zone suggests that the concentration of W was depleted near the tempered-martensite/δ-ferrite grain boundary. The depletion of W near such interfaces is probably caused by the precipitation of W-rich M_6C at the interphase boundary during tempering.

The precipitation of Fe_2W noticeably increases the amount of extracted residues. In Figure 7, the amount of extracted residues from the 9Cr-4W steel after aging at 873 K for 3600 ks is larger than that expected (shown by the extrapolated dotted line) from similar extractions from steels with less W aged at the same conditions. The increase in the amount of extracted residues due to aging was the same for the 9Cr, 9Cr-1W, and 9Cr-2W steels and resulted from additional precipitation of $M_{23}C_6$ during aging. Therefore, the amount of precipitates as a function of W concentration of these steels remained linear, even after aging. On the other hand, as described earlier, only $M_{23}C_6$ and M_6C carbides were present after tempering with no Fe_2W in the 9Cr-4W steel, and the increase in the amount of extracted residues with W concentration up to 4 pct W was fairly linear. This appears due to mainly the extra precipitation of Fe_2W Laves phase in the 9Cr-4W steel in addition to carbides present, although the ratio of $M_6C/M_{23}C_6$ may also change during

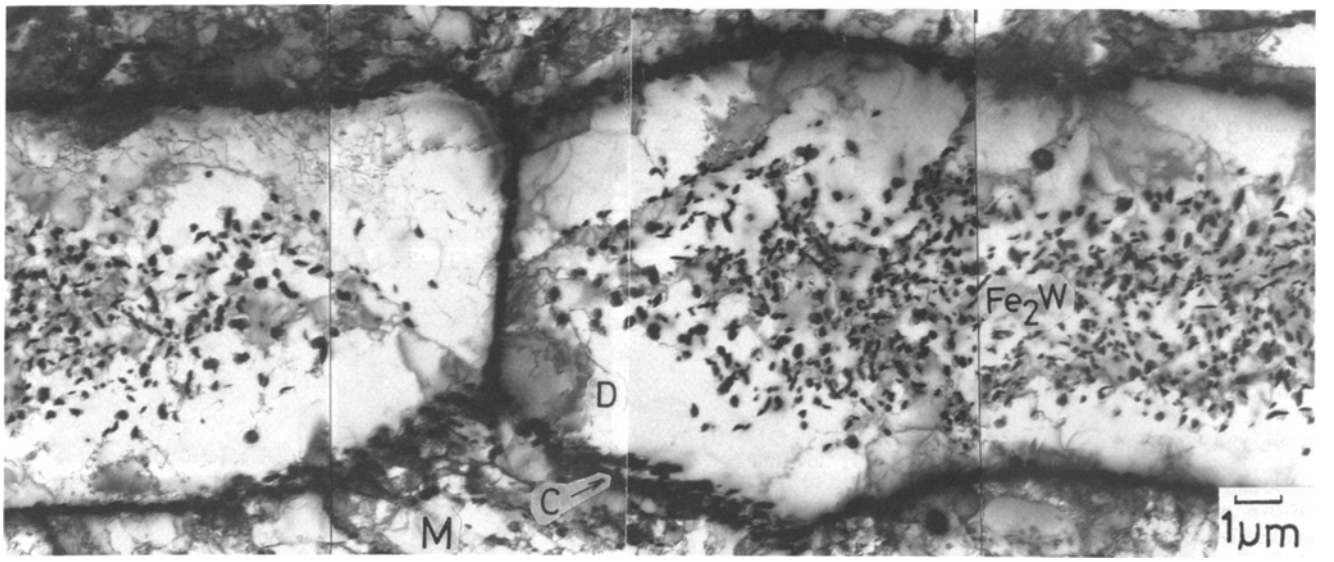

Fig. 11—The δ-ferrite phase of 9Cr-4W steel after aging at 873 K for 3600 ks. The precipitates in the δ-ferrite were identified as Fe_2W. The symbols "C," "D," and "M" in the micrograph denote carbides at the tempered-martensite/δ-ferrite interface, Fe_2W-denuded zone, and tempered-martensite phase, respectively.

aging in the 9Cr-4W steel and may affect the increased amount of extracted residues.

Figure 13 shows the microstructural evolution due to the precipitation of Fe_2W Laves phase in the δ-ferrite phase of the 9Cr-4W steel during aging. The most extensive precipitation of Fe_2W occurred at 923 K. At 923 K, the Fe_2W Laves particles of about 0.1 μm were observed after 36 ks, corresponding to nucleation stage, and they grew to 0.5 to 1 μm in size after 3600 ks. With decreasing aging temperature, the size of the precipitates decreases, suggesting a decrease in growth rate, but the number density increases at lower aging temperatures, indicating an increased nucleation rate. As can be seen from the microstructure after 823 K-3600 ks and 873 K-360 ks, the Fe_2W precipitates appear as small thin disks in the initial stage of precipitation. As precipitation progresses, the growth of the precipitates occurs in both thickness and radial directions, resulting in the massive precipitates seen in the microstructure after 923 K-3600 ks. On the other hand, at 973 K, there is no evidence for Fe_2W precipitation, indicating that W is soluble in the δ-ferrite at this temperature. Figure 14 shows the temperature-time-precipitation (TTP) curve for Fe_2W, which was derived from the results in Figure 13. The nose of the TTP curve is located at 923 K and 20 to 30 kiloseconds.

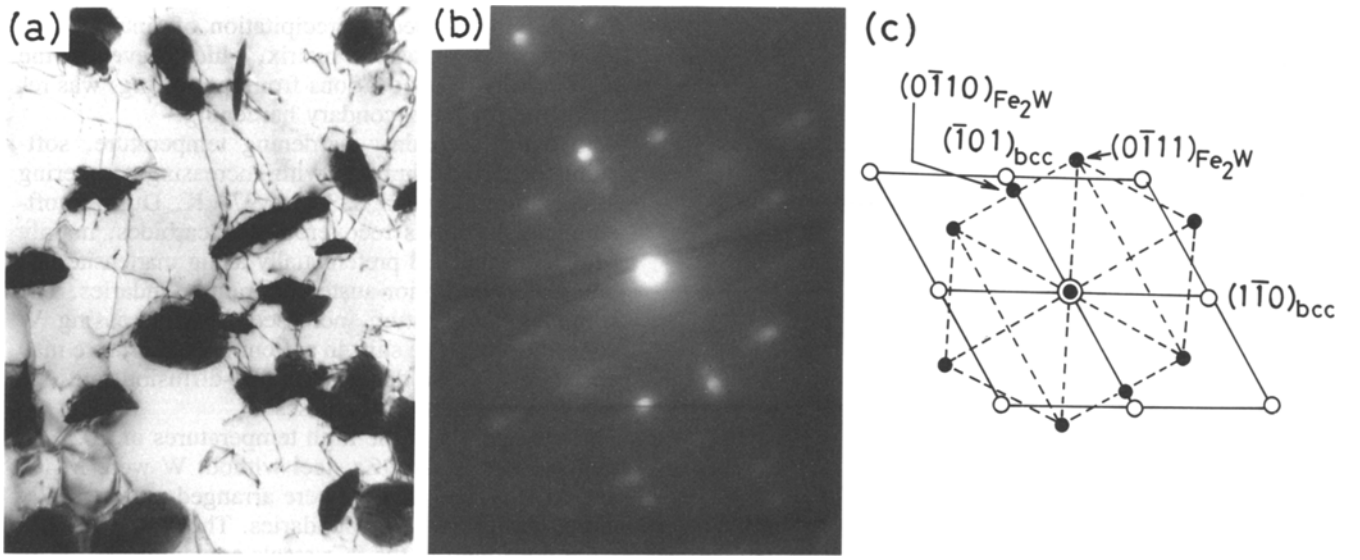

Fig. 12—Selected area diffraction of Fe_2W precipitates in 9Cr-W aged at 873 K for 3600 ks: (*a*) bright-field image, (*b*) selected area diffraction pattern, and (*c*) key diagram of (b).

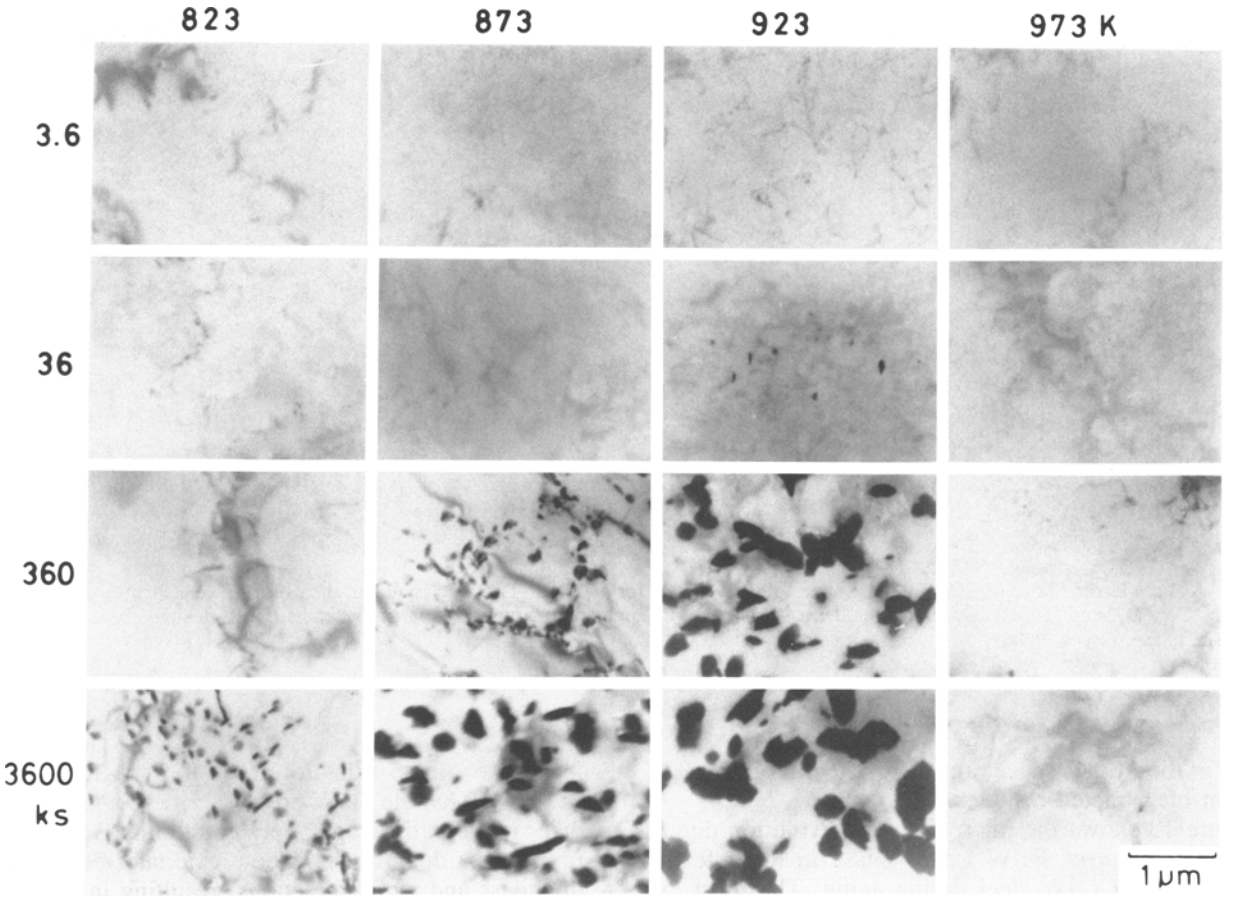

Fig. 13—Series micrographs of Fe_2W precipitation in δ-ferrite of 9Cr-4W.

IV. SUMMARY

The effect of W on the dislocation recovery and precipitation behavior in martensitic 9Cr-W-0.1C steels with 0, 1, 2, and 4 pct W was investigated after quenching, tempering, and subsequent prolonged aging. The main results are summarized as follows.

1. The 9Cr, 9Cr-1W, and 9Cr-2W steels were fully martensitic, with lath subgrains containing a high density of dislocations. The addition of 4 pct W caused the formation of some δ-ferrite during austenitizing, which produced δ-ferrite plus martensite after cooling. The δ-ferrite grains contained quite a low density of dislocations. The critical concentration of W for δ-ferrite formation was estimated to be about 3 pct.
2. The steels containing W exhibited secondary hardening at tempering temperatures between 673 and 823 K. Homogeneous precipitation of fine W_2C in the tempered-martensite matrix, which prevented the high density of dislocations from recovering, was responsible for the secondary hardening.
3. Above the secondary hardening temperature, softening occurred abruptly with increasing tempering temperature between 823 and 973 K. During softening, dislocations recovered, and carbides, mainly $M_{23}C_6$, precipitated preferentially along martensite lath boundaries and prior austenite grain boundaries. The softening temperature increased with increasing W concentration. The shift in softening temperature may correlate with the decrease in self-diffusion rates, as the W concentration increases.
4. After tempering at the high temperatures of 1023 K, the carbides in the 9Cr steel without W were $M_{23}C_6$ and M_7C_3. The carbides were arranged preferentially along martensite lath boundaries. The M_7C_3 carbides were not found in the 9Cr steels containing W. With less than 2 pct W, the 9Cr steel contained $M_{23}C_6$ and, with 4 pct W, contained M_6C and $M_{23}C_6$.

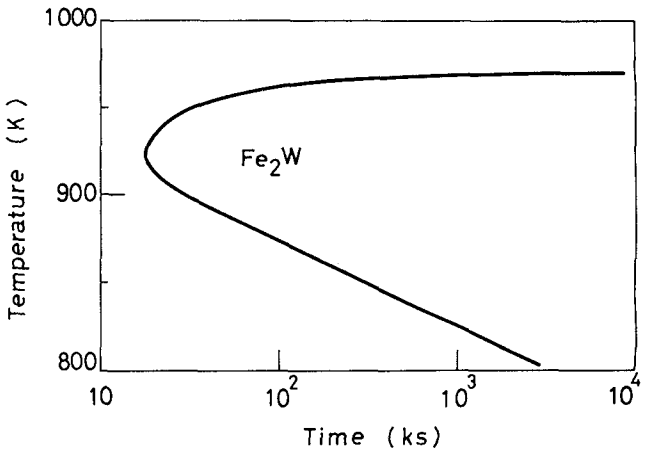

Fig. 14—TTP diagram of Fe_2W in 9Cr-W.

5. After tempering, prolonged aging at temperatures between 823 and 973 K produced agglomeration of the carbides, further recovery of the dislocations, and growth of martensite lath subgrains. The rates of these components of the microstructural evolution increased with increasing aging temperature and with decreasing W concentration. The as-tempered M_7C_3 carbides in the 9Cr steel dissolved and were replaced during aging by more stable $M_{23}C_6$. The Fe_2W Laves phase formed in the δ-ferrite grains, which were W-enriched, during aging of the 9Cr-4W steel. The nose of the Fe_2W phase TTP diagram was located at 923 K and 20 to 30 kiloseconds.

REFERENCES

1. D.S.Gelles: in *Optimizing Materials for Nuclear Applications*, F.A. Garner, D.S. Gelles, and F.W. Wiffen, eds., TMS-AIME, Warrendale, PA, 1985, pp. 63-71.
2. R.L. Klueh and E.E. Bloom: *Nucl. Eng. Des./Fusion*, 1985, vol. 2, pp. 383-89.
3. T. Noda, F. Abe, H. Araki, and M. Okada: *J. Nucl. Mater.*, 1986, vol. 141–143, pp. 1102-06.
4. D.S. Gelles and M.L. Hamilton: *J. Nucl. Mater.*, 1987, vol. 148, pp. 272-78.
5. R.L. Klueh and P.J. Maziasz: *J. Nucl. Mater.*, 1988, vol. 155–157, pp. 602-07.
6. F. Abe, T. Noda, H. Araki, M. Narui, and H. Kayano: *J. Nucl. Mater.*, 1989, vol. 166, pp. 265-77.
7. R.L. Klueh and P.J. Maziasz: *Metall. Trans. A*, 1989, vol. 20A, pp. 373-82.
8. R.D. Griffin, R.A. Dodd, G.L. Kulcinski, and D.S. Gelles: *Metall. Trans. A*, 1990, vol. 21A, pp. 1853-61.
9. F. Abe, H. Araki, and T. Noda: *Mater. Sci. Technol.*, 1990, vol. 6, pp. 714-23.
10. F. Abe, H. Araki, T. Noda, and M. Okada: *J. Nucl. Mater.*, 1988, vol. 155–157, pp. 656-61.
11. G.V. Raynor and V.G. Rivlin: *Int. Met. Rev.*, 1983, vol. 28, pp. 122-29.
12. Yu.I. Ustinovshchikov: *Met. Sci.*, 1984, vol. 18, pp. 337-44.
13. A.W. Bowen and G.M. Leak: *Metall. Trans.*, 1970, vol. 1, pp. 2767-73.
14. J. Cermak, J. Kucera, B. Million, and J. Krumpos: *Kov. Mater.*, 1980, vol. 18, pp. 537-47.
15. J.W. Christian: *Theory of Transformation in Metals and Alloys*, Pergamon Press, Oxford, United Kingdom, 1965, pp. 670-709.
16. F. Abe, T. Noda, H. Araki, and M. Okada: in *Reduced Activation Materials for FUSION REACTORS*, R.L. Klueh, D.S. Gelles, M. Okada, and N.H. Packan, eds., ASTM-STP-1047, ASTM, Philadelphia, PA, 1990, pp. 130-39.
17. Y. Hosoi, N. Wade, S. Kunimitsu, and T. Urita: *J. Nucl. Mater.*, 1986, vol. 141–143, pp. 461-67.